ACS APPLIED MATERIALS & INTERFACES

Research Article

www.acsami.org

Tattoolike Polyaniline Microparticle-Doped Gold Nanowire Patches as Highly Durable Wearable Sensors

Shu Gong,[†] Daniel T.H. Lai,[§] Yan Wang,[†,‡] Lim Wei Yap,[†,‡] Kae Jye Si,[†,‡] Qianqian Shi,[†,‡] Naveen Noah Jason,[†,‡] Tam Sridhar,[†] Hemayet Uddin,[‡] and Wenlong Cheng*[,†,‡]

[†]Department of Chemical Engineering, Monash University, Clayton, Victoria 3800, Australia

[‡]The Melbourne Centre for Nanofabrication, 151 Wellington Road, Clayton, Victoria 3800, Australia

[§]College of Engineering and Science, Victoria University, Melbourne, Victoria 8001, Australia

Supporting Information

ABSTRACT: Wearable and highly sensitive strain sensors are essential components of electronic skin for future biomonitoring and human machine interfaces. Here we report a low-cost yet efficient strategy to dope polyaniline microparticles into gold nanowire (AuNW) films, leading to 10 times enhancement in conductivity and ∼8 times improvement in sensitivity. Simultaneously, tattoolike wearable sensors could be fabricated simply by a direct "draw-on" strategy with a Chinese penbrush. The stretchability of the sensors could be enhanced from 99.7% to 149.6% by designing curved tattoo with different radius of curvatures. We also demonstrated roller coating method to encapusulate AuNWs sensors, exhibiting excellent water resistibility and durability. Because of improved conductivity of our sensors, they can directly interface with existing wireless circuitry, allowing for fabrication of wireless flexion sensors for a human finger-controlled robotic arm system.

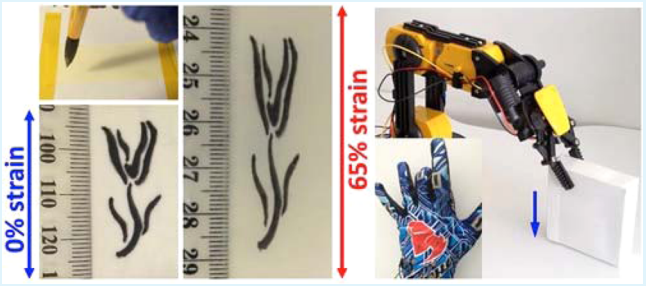

KEYWORDS: *ultrathin gold nanowires, polyaniline, electronic skin, strain sensor, wearable*

Stretchable and highly sensitive strain and flexion sensors have received tremendous attention due to their potential applications in wearable electronics,[1−9] biomonitoring,[10−13] and human/machine interface.[14−16] The key challenge in designing such sensors is to achieve reasonably high stretchability without materials delamination, while maintaining excellent sensing performance. Traditional metal-based strain gauges are brittle (Young's modulus > 1×10^{10} Pa) with limited stretchability (ε < 5%),[17] which cannot meet the pressing demand for the above-mentioned applications, such as wearable biomedical sensors for health monitoring anytime anywhere.

A promising strategy to future ultimate wearable sensors is to use electronic skin (e-skin) materials by integration of optoelectronically active nanomaterial with polymeric elastomers.[5,10,18−28] To date, a variety of nanomaterials, including zero-dimensional (0D) nanoparticles (NPs),[18,19] one-dimensional (1D) nanowires (NWs)[20−23]/carbon nanotubes (CNTs),[5,10,24] and two-dimensional (2D) graphene[25−29] have been used in the design of e-skin materials-based sensors. Despite the success, these single-component e-skins have limitations. For example, 0D NP-based e-skins could achieve an extremely high sensitivity (gauge factor (GF) > 100),[18] but they exhibited limited stretchability due to the irreversible changes in interparticle gaps under large strains. However, 1D nanomaterials-based systems could achieve extremely high stretchability but often exhibit poor sensitivity (GF < 10).[20−24] In this context, binary systems of 0D and 1D has been explored, including CNTs/AgNPs,[30] CNTs/graphene,[31,32] and AgNWs/AgNPs.[33] It was reported that the sensitivity could increase more than 23 times when silver NPs were added into CNTs;[30] the conductivity could increase more than 1×10^6 times when AgNPs were added into AgNWs.[33]

Recently, we successfully fabricated wearable pressure sensors[13] and highly stretchable strain sensors[20] using ultrathin gold nanowires (AuNWs). Unlike other 1D nanomaterials, which are straight with high persistence length, AuNWs are serpentine at the nanoscale behaving like "polymer chains" due to their ultrathin nature (2 nm in width, with an aspect ratio > 10 000).[34−36] Hence, the AuNWs are intrinsically stretchable, which have been demonstrated to be a unique e-skin material for stretchable electronics.[20,34−36] However, one limiting factor for pristine AuNWs films is that their conductivity remains low, preventing their direct integration with existing miniaturized wireless circuitry, which often requires a resistance of KΩ. Herein, we demonstrate a simple yet efficient approach to dope polyaniline (PANI) microparticles into AuNW films, leading to 10 times enhancement in conductivity allowing for direct integration with wireless circuitry to remotely control robotic

Received: June 6, 2015
Accepted: August 24, 2015
Published: August 24, 2015

DOI: 10.1021/acsami.5b05001
ACS Appl. Mater. Interfaces 2015, 7, 19700−19708

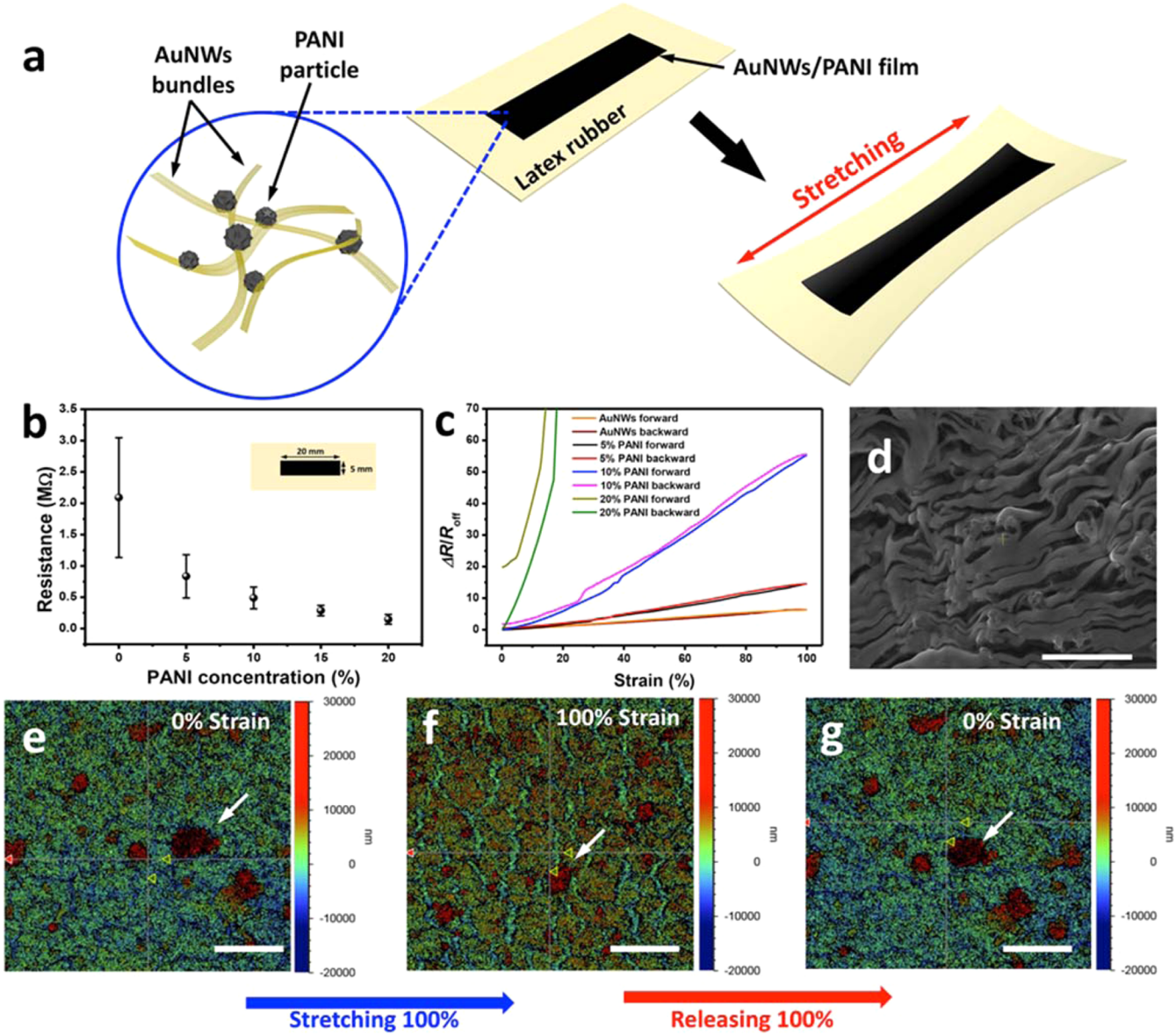

Figure 1. (a) Schematic of the AuNWs/PANI strain sensors. (b) Plot of sheet resistance of AuNWs/PANI film at various PANI concentrations (w/w) from 0 to 20%. (c) Plot of resistance response as a function of strain for four AuNWs/PANI sensors with various PANI concentrations (w/w) (0%, 5%, 10%, and 20%). The linear stage moving speed was fixed to 2 mm/s for all tests. (d) SEM image of the surface morphology of AuNWs/PANI strain sensors (weight fraction of PANI: 10%) on latex rubber substrate (scale bar: 5 μm). (e–g) Optical profilometry images of a AuNWs/PANI strain sensor before stretching (e), under 100% stretching (f), and after releasing (g; scale bar: 100 μm).

arms. Simultaneously, ~8 times improvement in sensitivity was achieved. Moreover, tattoolike wearable sensors could be fabricated simply by a direct writing strategy with a Chinese penbrush. For the curved tattoo with different radius of curvatures, the stretchability could be enhanced from 99.7% to 149.6%. We also demonstrated roller-coating method to package AuNWs sensors, showing excellent water resistibility and durability.

RESULT AND DISCUSSION

The hybrid conductive ink was first prepared by mixing AuNW solution (10 mg/mL)[34−36] and PANI solution (10 mg/mL) with various ratios (w/w). After it was mixed and sonicated (10 min, 50 Hz), the composite mixture was ready for drop-casting or direct writing of desired patterns onto latex rubber substrate. Figure 1b shows the sheet resistance variation of the AuNWs/PANI films with respect to PANI concentrations (w/w, 0–20%) by drop-casting. The thickness of film was controlled at ~2 μm with 20 × 5 mm^2 patches confined by polyimide tape masks. The initial sheet resistance of AuNWs film without PANI was measured as 2.09 ± 0.95 MΩ and then gradually decreased according to the increase of PANI concentration before finally reaching 148.1 ± 78.2 kΩ at PANI concentration of 20%. The lower electrical resistance is mainly due to the presence of PANI microparticles (Figure S1), which reduced the resistivity by providing more connection points for conduction pathways.[30,33] Notably, the conductivity of the hybrid film can be further improved by continually increasing the PANI concentration. However, if PANI concentration was too high, the films were found to have macroscopic cracks after stretching (Figure S2), demonstrating the critical role of

DOI: 10.1021/acsami.5b05001
ACS Appl. Mater. Interfaces 2015, 7, 19700−19708

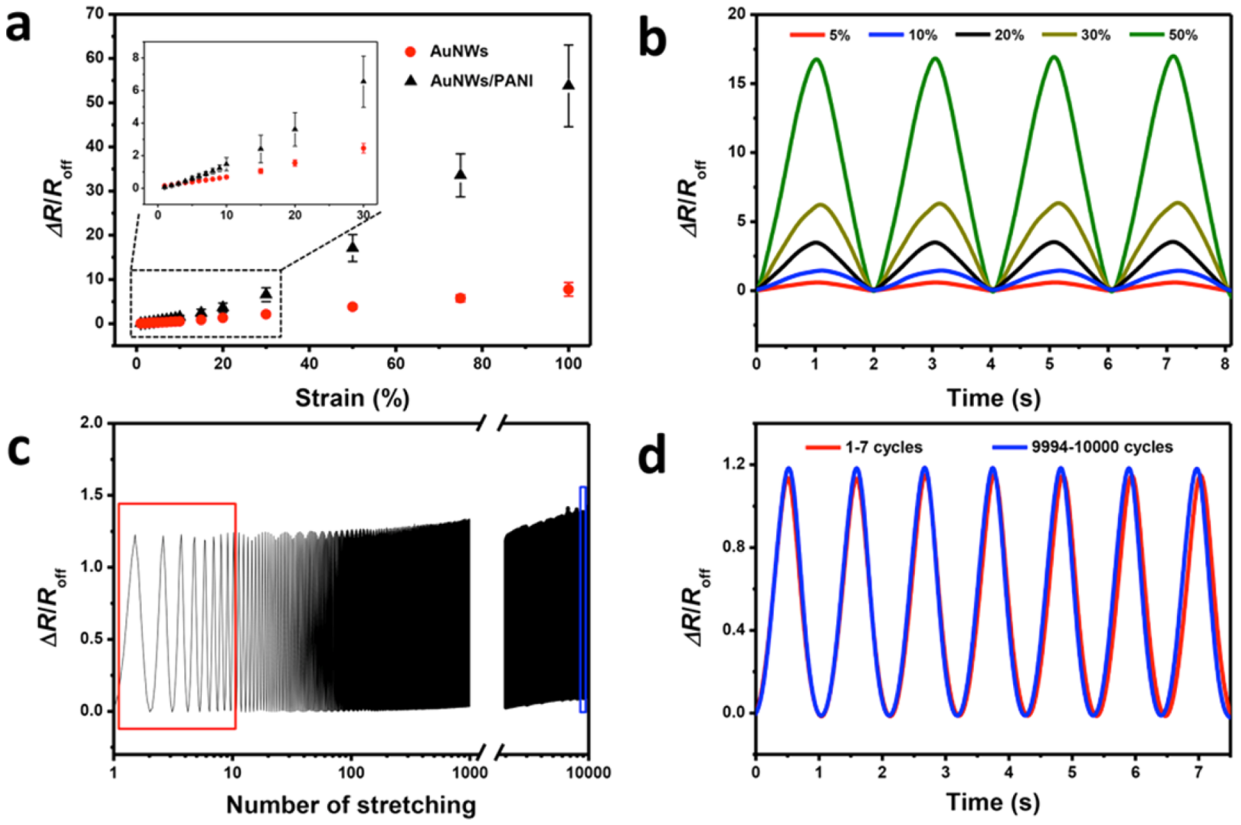

Figure 2. (a) Electrical resistance changes of AuNWs/PANI strain sensors in comparison with AuNWs strain sensors under various strains. (b) Plot of resistance response as a function of time (strain frequency: 0.5 Hz) for five applied strain (5%, 10%, 20%, 30%, and 50%). (c) The durability test under a strain of 5% for 10 000 cycles at a frequency of 1.05 Hz. (d) Enlarged view of the part of the $R-t$ curve in (c), red line represents the first seven cycles, and blue line represents the last seven cycles of the test.

AuNWs in the composite films for providing a conductive yet stretchable matrix.

In addition, we estimated the stretchability of four samples with PANI concentrations of 0%, 5%, 10%, and 20% by measuring the electrical resistance changes of each film at full-scale strain of 0%−100%−0% with a stage moving speed of 2 mm/s (Figure 1c). The results indicated that the resistance of hybrid film with PANI concentration ≤ 10% can be well-recovered after strain at 100%, but AuNWs−20%PANI film become nonconductive after strains of more than 20%, which resulted in irreversible resistance increase of ∼20 times after recovery. This is because higher loading of PANI microparticles led to brittleness of the hybrid film, which showed permanent breakage under large strain. Therefore, AuNWs−10%PANI film was chosen as the optimized weight ratio in the following analysis. The scanning electron microscopy (SEM) image (Figure 1d) of AuNWs−10%PANI film showed that the PANI microparticles were well-dispersed in the AuNWs bunches.

To investigate the working mechanism of our strain sensor, a full stretch−release cycle of an AuNWs−10%PANI film under strain of 0−100%−0 was recorded by in situ optical profilometry (Figure 1e−g; the white arrow indicates the same PANI particle). In these images, AuNWs and PANI microparticles are highly distinguishable as PANI microparticles are much higher than AuNWs thus showing various colors (green for AuNWs and red for PANI microparticles). As shown in Figure 1e, owing to much larger size of PANI microparticles, the hybrid film exhibited a sea−island morphology, and no cracks or gaps were observed before stretching. As strain increased to 100% (Figure 1f), cracks occurred and grew on the film. Note that almost all the cracks were generated between NWs, while most of the PANI microparticles remain intact. This is attributed to the sea−island structure, in which soft and elastic AuNWs matrix can absorb reversibly external forces and stretch reversibly, but brittle PANI microparticles are unaffected by deformation. The cracks are responsible for the decrease of conductive pathways, which increases the overall electrical resistance. Remarkably, the cracks self-repaired after the full strain recovery, and the relative location of PANI microparticles were unchanged (Figure 1g), indicating almost no conductivity changes after a full stretching cycle. The morphologies of AuNWs−10%PANI film under various strains (0%, 50%, 100%, and back to 0%) were characterized (Figure S3), which supported the above cracking and crack-repairing mechanism with and without strains. They also correlated with corresponding electrical resistance (Figure S3e).

Electrical resistance of AuNWs−10%PANI composite films as a function of mechanical strain was shown in Figure 2a (black triangle). The strain sensitivity in the composite film is evaluated by GF, which is defined by the ratio of relative resistance change and strain as

$$\mathrm{GF} = (R - R_{\mathrm{off}})/R_{\mathrm{off}}\varepsilon \quad (1)$$

where ε is the strain, and R_{off} is electrical resistance under no strain. A GF of 20.4 was obtained in the low-strain range (0−30%), whereas GF increased to ∼61.4 at large strain of 100%. In comparison, a typical GF of 6.9−9.9 is obtained by AuNWs only (red circle), which is more than 8 times smaller than the

DOI: 10.1021/acsami.5b05001
ACS Appl. Mater. Interfaces 2015, 7, 19700−19708

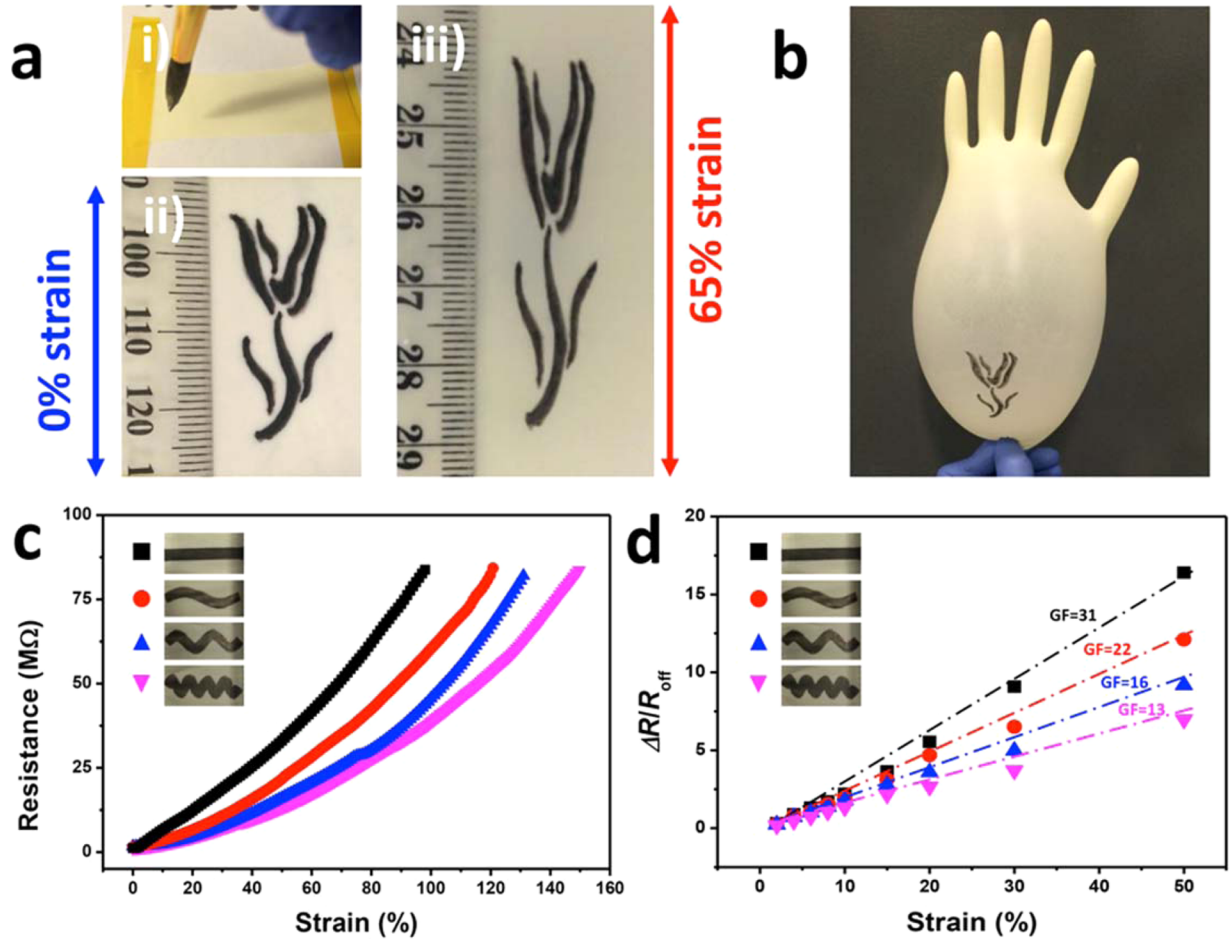

Figure 3. (a) Photograph of the direct-writing process: (i) Writing AuNWs/PANI film by using painting brush. (ii) Photograph of a "rose" pattern of AuNWs/PANI film. (iii) Photograph of the "rose" pattern under 65% uniaxial strain. (b) Photograph of the rose-patterned glove after inflated with air. (c) The stretchability test for four AuNWs/PANI sensors with different sine curve patterns. The electrical resistance was measured as a function of strain for sensors strained to electrically not conductive (stage moving speed 2 mm/s). (d) The electrical resistance changes under various strains (0−50%) for four AuNWs/PANI sensors with different sine curve patterns. GF could be derived by linear fitting.

hybrid film under large strain. This could be attributed to PANI-enhanced cooperative conductivity.[30] The presence of PANI microparticles enhanced the percolation conductivities of NW networks because they provided more connection points for electron-transport pathways. However, this high conductivity is more vulnerable to nanowire film crack, which could cause "sudden" decrease in conductivity. The high−low conductivity switching may be responsible for the substantially high sensitivity obtained for our hybrid films.

The electrical responses of the sensors as a function of dynamic strain was measured in Figure 2b, where five strains varied from 5% to 50% were applied. A proportional relation between resistance changes and applied strain was obtained with high repeatability. In addition, the stable performance of the sensor under static strain was also demonstrated by the current−voltage (I−V) measurement (Figure S4).

To further examine the mechanical durability of the AuNW/PANI sensors, the resistance changes of the film were monitored under a cyclic strain of 0%−5%−0% at a fixed frequency of 1.05 Hz (Figure 2c). As indicated by Figure 2d, the strain sensor shows no measurable change of electrical properties after 10 000 continuous stretching−releasing cycles and long working hours (∼3 h), exhibiting excellent reproducibility and durability.

Interestingly, the AuNWs/PANI ink could be delivered directly by a Chinese penbrush. As illustrated in Figure 3a, a "rose" pattern with size of 30 × 8 mm^2 was written on latex glove, which was capable of stretching (65% uniaxial strain, Figure 3a) and expanding (Figure 3b). To further investigate how topological patterns affect sensing performance, we designed and fabricated sine-wave patterns (Figure 3c, inset) following the equation

$$y = A \sin(kx) \tag{2}$$

where y is the full contour height of the curve, x is the length, A is the amplitude, and k is the pattern parameter. In our case, we selected x at the section of 0−30 mm. The line width, length, and thickness of the patterns were kept at 5 mm, 30 mm, and 2 μm, respectively. We compared the four sensors by setting k equal to 0, π/15, 2π/15, and 4π/15.

To estimate the upper strain limit, all the sensor strips were stretched at a moving speed of 2 mm/s until conductivity was lost (Figure 3c; ∼20 prestretching cycles were performed to stabilize the base resistance before the failure test). The prestretching process resulted in irreversible changes in film surface morphologies (Figure S5a,b). However, the surface features could be fully recovered after stretch released even after 1000 cycles[5,10] (Figure S5a−c). This explained the

DOI: 10.1021/acsami.5b05001
ACS Appl. Mater. Interfaces 2015, 7, 19700−19708

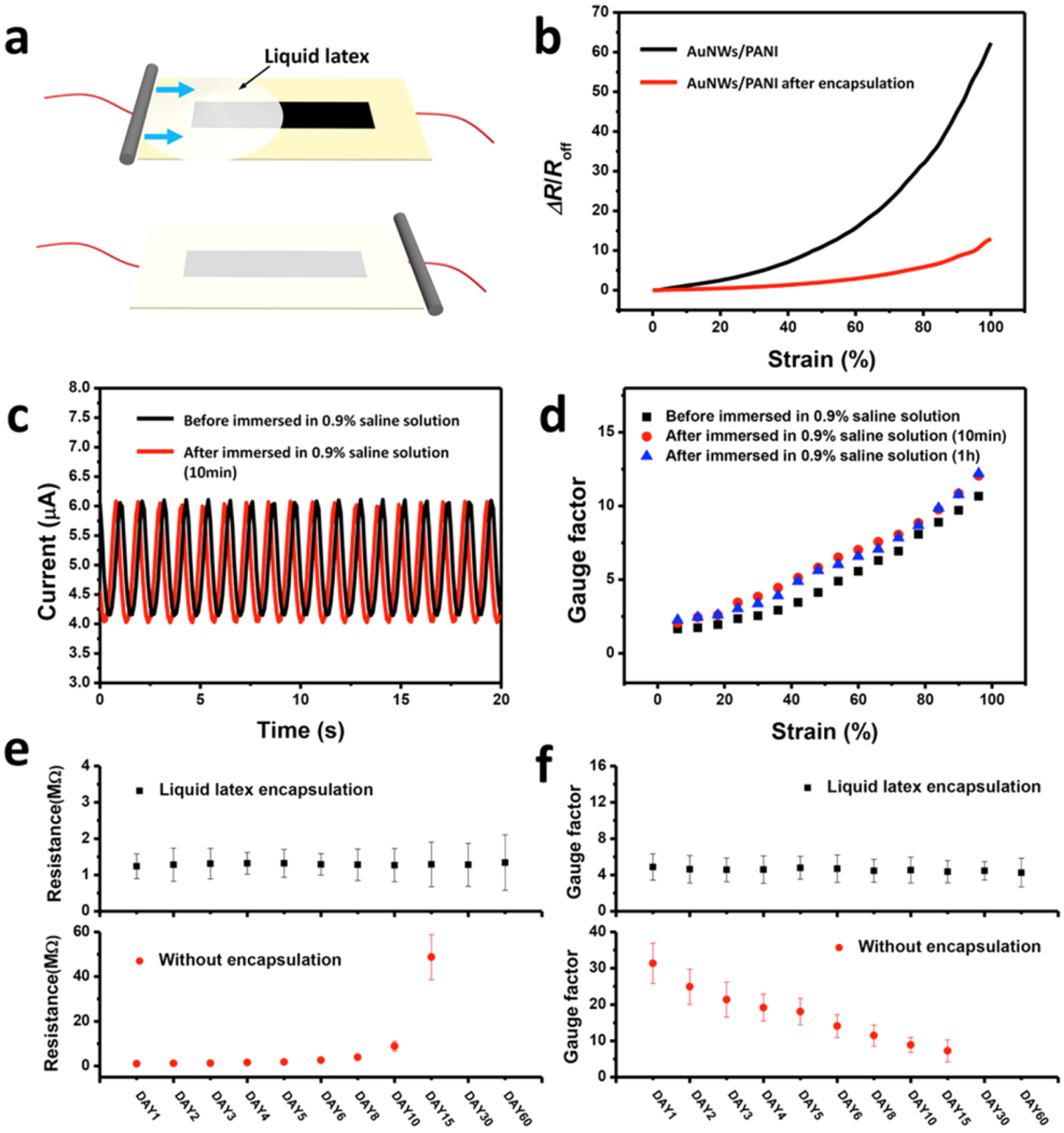

Figure 4. (a) Scheme of the liquid latex encapsulation process. (b) Plot of resistance response as a function of strain for AuNWs/PANI strain sensors before (black line) and after encapsulation. (c) The current changes of the encapsulated sensor under dynamic strain of 0−20%−0 before (black line) and after immersed in 0.9% saline solution for 10 min. (d) GFs changes of the sensor from 0 to 100% before and after immersed in 0.9% saline solution with various time. (e) Long-term stability of electrical resistance of the sensor under no strain before (red) and after (black) encapsulation. (f) Long-term stability of GF of the sensor under 50% strain before (red) and after (black) encapsulation.

excellent durability and low hysteresis of our strain sensor after prestretching steps. As expected, an electrical disconnection of linear AuNWs/PANI film occurred at a 99.7% strain. In contrast, the maximum strains at which the curved patterns did not lose their electrical conductivity significantly increased to 120.8%, 131.0%, and 149.6%, corresponding to $k = 0$, $\pi/15$, $2\pi/15$, and $4\pi/15$, respectively. This can be attributed to the facts that curved patterns have larger surface area per unit length than linear patterns and are able to absorb more strains. However, the structural deformation per unit length of curved strips is much smaller when compared to linear strip, resulting in a decrease in GFs (Figure 3d). The effects of GF on pattern curvature were shown in Figure S6, and they could be explained well by the curvature-dependent mechanics model.[37] Our results indicate that more complex patterns could be fabricated with our strategy, leading to wearable tactile sensors specifically recognizing local stress/strains of skins or muscles. The stretchability of our AuNWs/PANI sensors could be further enhanced by a prestretching strategy. After prestretching latex rubber of 50% before AuNWs/PANI ink deposition, the stretchability of the composite sensors could reach 200% without much sacrifice of sensitivity (Figure S7).

Our hybrid conductive ink could be potentially printed or patterned by other approaches such as ink jet printing. To demonstrate this, we show that the viscosity of our ink could be easily tuned from 1.04 to 44.1 mPa·s simply by changing the

DOI: 10.1021/acsami.5b05001
ACS Appl. Mater. Interfaces 2015, 7, 19700−19708

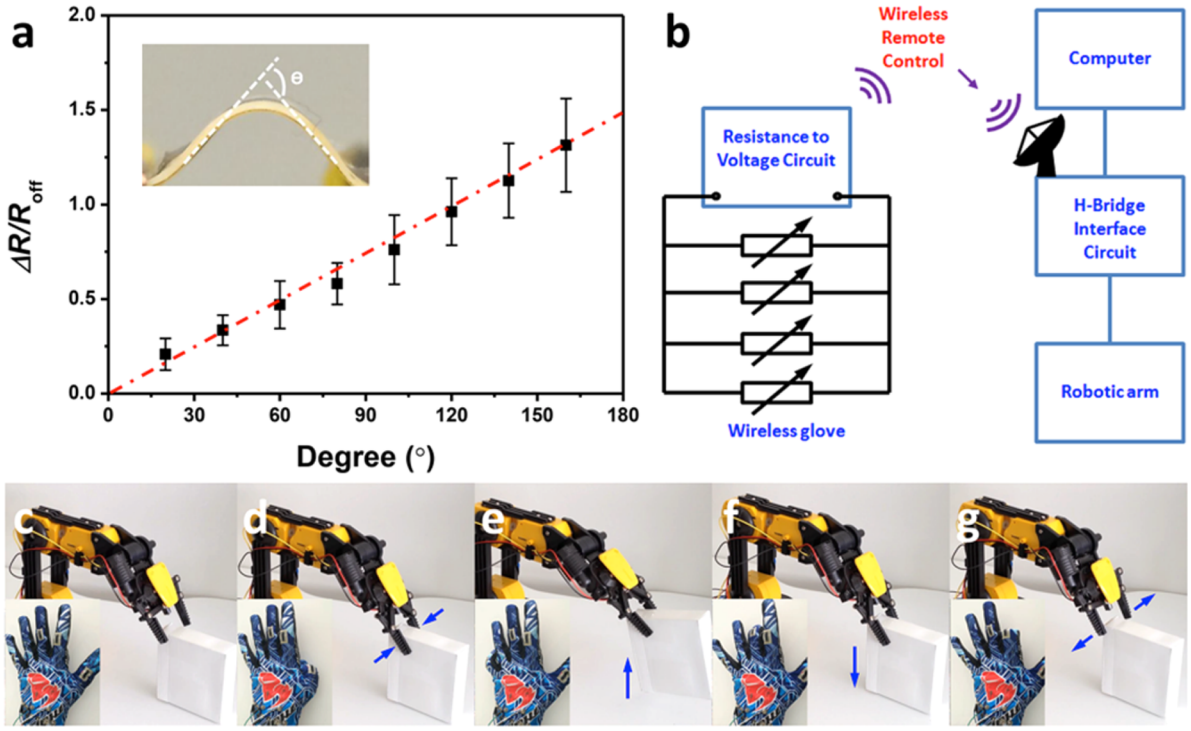

Figure 5. (a) Plot of resistance response as a function of bending degree for the flexion sensors. (b) Schematic diagram of the remote controlling configuration. (c–g) The whole process of the remote controlling performance of four flexion sensors sewed on a textile glove. Relaxed state (c) → clamping object (d) → lifting object up (e) → putting object down (f) → releasing object (g).

concentration of AuNWs from 2%–12% (w/w; Figure S8). This meets the viscosity requirement in ink jet printable materials inks (Table S1).

Furthermore, we developed a simple yet efficient encapsulation method to fabricate water-resistant sensors with high durability. As shown in Figure 4a, a thick solution of liquid latex was first spread onto surface of the AuNW/PANI film. Then the latex solution was uniformly coated by rolling a cylinder-shaped metal bar from one edge to another. After 30 min, a transparent and stretchable thin film (~50 μm) formed on the AuNWs/PANI sensor (Figure S9b, inset), which was confirmed by cross-sectional SEM images (Figure S9). The encapsulation layer exhibited strong adhesion with the bottom sensor patches even under large strain (Figure S10). This is attributed to the fact that the encapsulation materials have similar chemical composition with latex rubber substrates. After encapsulation, the sensitivity decreased (Figure 4b), which may be due to the prevention of islands and gaps formed under high strains (Figure S11). Without latex sealing, the strain-induced formation of islands and gaps (Figure S11b) is responsible for the decrease of conductive pathways; however, after encapsulation with latex, no apparent islands and gaps were observed under similar strains (Figure S11e). This explains why a smaller bulk resistance changes compared to sensors without encapsulation.

To evaluate water resistivity of our sensor for bio-related application,[38] the current changes under dynamic strain (0–20%-0) were measured before and after dipping sensors into 0.9% saline solution for 10 min. As indicated in Figure 4c, the sensor exhibited negligible changes in current amplitude and remained highly stable after immersion into 0.9% saline solution. In addition, the full-range (0–100%) sensitivity of the sensor was measured with various soak time (10 min, 1 h, Figure 4d). The GFs of our device did not show evident changes with soak time of 10 min and 1 h.

Latex-sealed sensors showed exceptional long-term stability. Figure 4e showed the base electrical resistance changes of the devices with (black rectangle) or without encapsulation (red circle) during 60 d (both sensors were stored in a Petri dish at ambient conditions). All the specimens without encapsulations exhibited large shift of base resistance after 15 d and became completely insulative after 30 d. In contrast, the base resistance of encapsulated sensors showed negligible changes even after 60 d. Simultaneously, the sensitivity of encapsulated sensors was unchanged (measured strain at 50%), while unencapsulated sensors suffered from more than 300% GF degeneration after 15 d.

The conductivity of our highly durable sensors could be tuned to match the requirement in existing wireless circuitry. This allowed us to fabricate flexion sensors to be used in robotic arms. Figure 5a illustrates the sensing responses of the sensor as a function of applied bending degree. A linear electrical resistance ($(\Delta R/R_0/\theta) \approx 0.83$ rad^{-1}) was observed corresponding to a full range of bending stepping from 0° to 160°. The highly distinguishable signals of the AuNWs strain sensors responding to strain and bending enabled their potential applications as wearable devices for real-time remote controlling. To demonstrate this potential, we designed and fabricated a smart glove system to remotely control a robotic arm by encapsulated AuNWs/PANI sensors via wireless signals. Figure 5b shows schematic diagram to realize remote controlling. In details, the smart glove was integrated with a custom written graphical user interface (GUI) with a Bluetooth radio (SENA Parani ESD200) on a chip. The designed chip acquired response data from each sensor and transmitted the data to a computer wirelessly. Then the wireless signals were used to activate the respective motors in the robot arm based

DOI: 10.1021/acsami.5b05001
ACS Appl. Mater. Interfaces 2015, 7, 19700–19708

on a thresholding algorithm. There are two motors (gripper motor and elbow motor) corresponding to four actions (gripper open/close, elbow up/down) that can be individually controlled by four different finger motions (the thumb finger: "gripper close", the index finger: "gripper open", the middle finger: "elbow down", the little finger: "elbow up"). As demonstrated in Figure 5c–g and Supplementary Movie 1, the robotic arm could be controlled wirelessly with our sensor-integrated glove.

CONCLUSION

In summary, we demonstrated a simple yet efficient "draw-on strategy" to fabricate wearable sensor patches and arbitrary tattoolike patterns using ultrathin gold nanowires and PANI microparticles. The binary AuNWs/PANI system possesses a unique sea–island structure allowing substantial improved conductivity (>8 times in sheet resistance) and sensitivity (GF increased by up to 8 times) in comparison to the sensors without PANI particles. After latex encapsulation, our sensors were fully water-resistant, exhibiting long-term durability. Because of wide-range tunability of our sensors, they can directly interface with existing wireless circuitry, allowing for fabrication of wireless flexion sensors for a human finger-controlled robotic arm system.

EXPERIMENTAL SECTION

Synthesis of Ultrathin Au Nanowires. Ultrathin AuNWs were synthesized following protocol reported previously.[36] At first, $HAuCl_4 \cdot 3H_2O$ (220 mg) was added in hexane (200 mL), followed by addition of oleylamine (OA, 7.5 mL) and triisopropylsilane (TIPS, 10 mL). Note that the gold salts were not dissolved until the addition of OA, which acted as a phase-transfer reagent. The resulting solution was left to stand for 2–3 d without stirring at room temperature until the color turned from yellow into dark red, indicating the formation of AuNWs. The residual chemicals were removed by repeated centrifugation, thorough washing by ethanol/hexane (3/1, v/v), and finally concentrated to a stock concentration of 10 mg/mL in hexane for further uses.

Mixing of Au Nanowires and Polyaniline Solution. PANI conductive powder (emeraldine salt, long chain, grafted to lignin) was dissolved in ethanol at a stock concentration of 10 mg/mL. The solution was then sonicated (Unisonics Austratlia, 50 Hz) for 30 min to be well-dispersed. Finally the AuNWs solution (10 mg/mL) and PANI solution (10 mg/mL) were mixed with tunable component concentrations.

Strain Sensor Fabrication. The strain sensor was fabricated either by directly writing or drop-casting. For the direct-writing process, frame of desired patterns was drawn on latex rubber with ball-point pen prior to depositing AuNWs/PANI ink. A Chinese penbrush was then dipped into AuNWs/PANI ink followed by carefully writing within pattern frames. After the solution was dried, the hybrid film is ready for further wiring. With the drop-casting process, latex rubber was first attached on a glass slide and patterned with polyimide masks (20×5 mm^2 rectangular pattern size). Then concentrated AuNWs/PANI ink was drop-casted onto the soft substrates and dried in fume cupboard. The wiring process is beginning at depositing silver paste (Sigma-Aldrich) onto both ends of the AuNWs/PANI strips connected with flexible conductive threads (Adafruit Industries). After the silver paste was dried (100 °C for 10 min on hot plate), polyvinyl alcohol glue (Craft Glue) was deposited on top of silver paste and dried in ambient condition (30 min), which permanently sealed the AuNWs/PANI film to conductive thread.

Encapsulation. A thick solution of liquid latex (~2 mL, Dalchem sprayable latex) was spread onto surface of the hybrid sensor. Then the latex solution was uniformly coated by rolling a cylinder-shaped metal bar from one edge to another. After 30 min of solvent evaporation, a transparent and stretchable thin film (~50 μm) was covered onto the AuNWs/PANI sensor.

Glove Sensors Fabrication. Four encapsulated AuNWs/PANI strain sensors were fabricated by the method demonstrated above. Then we use a needle and cotton threads to sew the strain sensors with each finger of a Thor Void Plus glove. The change of resistance in the strain sensors was then converted to analog voltage using a noninverting amplifier configuration. Analog voltage was converted to 10 bit digital samples using a Freescale 8-bit microcontroller (MC9S08SH8) sampling at 20 Hz. Data were sent wirelessly using bluetooth radio (SENA Parani ESD200) to a custom written GUI developed in Matlab 2014 (Mathworks Inc). The GUI also connected to an Arduino board (via USB), which controlled the motors in the robot arm via two dual H-Bridge drivers (L298N STMicroelectronics). Strain data from each finger was then used to activate the respective motors in the robot arm based on a thresholding algorithm.

Device Characterization. Scanning electron microscopy (SEM) images were characterized using an FEI Helios Nanolab 600 FIB-SEM (operating voltage of 5 kv and current of 86 pA). The surface profiles/morphology of AuNWs/PANI film were measured using a Bruker ContourGT-I 3D optical profilemeter (Karlsruhe, Germany). Optical images were taken by a Nikon ECLIPSE LV150 microscope with a Nikon Digital Sight DS-Fi1 camera. The sheet resistances of AuNWs film on latex rubber were performed on a Jandel four-point conductivity probe by using a linear arrayed four-point head. To test the strain-sensing characteristics, two ends of the samples were attached to motorized moving stages (THORLABS model LTS150/M), and then uniform stretching/releasing cycles were applied to the samples with a computer-based user interface (Thorlabs APT user), while the current differences and the $I-V$ characteristics for the pressure sensor were recorded by the Parstat 2273 electrochemical system (Princeton Applied Research). For the characterization of the bending angle detection by the strain sensors, a polyimide layer was attached under latex rubber substrate to ensure the accurate measurement of the bending angle.

Materials. Gold(III) chloride trihydrate ($HAuCl_4 \cdot 3H_2O$, ≥99.9%), triisopropylsilane (99%), and oleylamine were purchased from Sigma-Aldrich. Ethanol, hexane, and chloroform were obtained from Merck KGaA. All chemicals were used as received unless otherwise indicated. All glassware used in the following procedures was cleaned in a bath of freshly prepared aqua regia (***Caution!*** *Highly corrosive.*) and rinsed thoroughly in H_2O prior to use. Latex rubber was brought from MEDIflex industries.

ASSOCIATED CONTENT

Supporting Information

The Supporting Information is available free of charge on the ACS Publications website at DOI: 10.1021/acsami.5b05001.

SEM images of the AuNWs/PANI film, photographs of the strain sensor before and after stretching, SEM images of the AuNWs/PANI film under various strain, optical images and sheet resistance of the AuNWs/PANI film under various strain. $I-V$ curve of strain sensor at various tensile strains, SEM images of the AuNWs/PANI film before and after prestretching, the calculation of contour length of patterns and relationship between gauge factor and pattern parameter k, prestretched AuNWs/PANI strain sensors, the viscosity of AuNWs-10%PANI ink, The comparison of viscosity to other conductive printing materials, SEM images and photographs of the sensor before and after encapsulation, photographs of the sensor stretchability after encapsulation, optical images before and after encapsulation. (PDF)

Video illustrating the use of wearable sensors. (AVI)

DOI: 10.1021/acsami.5b05001
ACS Appl. Mater. Interfaces 2015, 7, 19700–19708

AUTHOR INFORMATION

Corresponding Author

*E-mail: wenlong.cheng@monash.edu. Phone: +61 399053147.

Notes

The authors declare no competing financial interest.

ACKNOWLEDGMENTS

This work is financially supported by ARC discovery Project No. DP120100170 and DP150103750. This work was performed in part at the Melbourne Centre for Nanofabrication in the Victorian Node of the Australian National Fabrication Facility. S.G. would like to thank the financial aid from Chinese Scholarship Council.

REFERENCES

(1) Kim, D.-H.; Lu, N.; Ma, R.; Kim, Y.-S.; Kim, R.-H.; Wang, S.; Wu, J.; Won, S. M.; Tao, H.; Islam, A.; Yu, K.; Kim, T. -i.; Chowdhury, R.; Ying, M.; Xu, L.; Li, M.; Chung, H. -J; Keum, H.; McCormick, M.; Liu, P.; Zhang, Y.-W.; Omenetto, F. G.; Huang, Y.; Rogers, J. A.; Coleman, T. Epidermal Electronics. *Science* **2011**, *333*, 838−843.

(2) Hammock, M. L.; Chortos, A.; Tee, B. C. K.; Tok, J. B. H.; Bao, Z. 25th Anniversary Article: The Evolution of Electronic Skin (E-Skin): A Brief History, Design Considerations, and Recent Progress. *Adv. Mater.* **2013**, *25*, 5997−6038.

(3) Kaltenbrunner, M.; Sekitani, T.; Reeder, J.; Yokota, T.; Kuribara, K.; Tokuhara, T.; Drack, M.; Schwödiauer, R.; Graz, I.; Bauer-Gogonea, S.; Bauer, S.; Someya, T. An Ultra-Lightweight Design for Imperceptible Plastic Electronics. *Nature* **2013**, *499*, 458−463.

(4) Takei, K.; Takahashi, T.; Ho, J. C.; Ko, H.; Gillies, A. G.; Leu, P. W.; Fearing, R. S.; Javey, A. Nanowire Active-Matrix Circuitry for Low-Voltage Macroscale Artificial Skin. *Nat. Mater.* **2010**, *9*, 821−826.

(5) Lipomi, D. J.; Vosgueritchian, M.; Tee, B. C.; Hellstrom, S. L.; Lee, J. A.; Fox, C. H.; Bao, Z. Skin-Like Pressure and Strain Sensors Based on Transparent Elastic Films of Carbon Nanotubes. *Nat. Nanotechnol.* **2011**, *6*, 788−792.

(6) Mannsfeld, S. C.; Tee, B. C.; Stoltenberg, R. M.; Chen, C. V. H.; Barman, S.; Muir, B. V.; Sokolov, A. N.; Reese, C.; Bao, Z. Highly Sensitive Flexible Pressure Sensors with Microstructured Rubber Dielectric Layers. *Nat. Mater.* **2010**, *9*, 859−864.

(7) Yi, F.; Lin, L.; Niu, S.; Yang, P. K.; Wang, Z.; Chen, J.; Zhou, Y.; Zi, Y.; Wang, J.; Liao, Q.; Zhang, Y.; Wang, Z. L. Stretchable-rubber-based Triboelectric Nanogenerator and Its Application as Self-Powered Body Motion Sensors. *Adv. Funct. Mater.* **2015**, *25*, 3688.

(8) Lin, L.; Xie, Y.; Wang, S.; Wu, W.; Niu, S.; Wen, X.; Wang, Z. L. Triboelectric Active Sensor Array for Self-powered Static and Dynamic Pressure Detection and Tactile Imaging. *ACS Nano* **2013**, *7*, 8266−8274.

(9) Someya, T.; Sekitani, T.; Iba, S.; Kato, Y.; Kawaguchi, H.; Sakurai, T. A Large-area, Flexible Pressure Sensor Matrix With Organic Field-Effect Transistors for Artificial Skin Applications. *Proc. Natl. Acad. Sci. U. S. A.* **2004**, *101*, 9966−9970.

(10) Yamada, T.; Hayamizu, Y.; Yamamoto, Y.; Yomogida, Y.; Izadi-Najafabadi, A.; Futaba, D. N.; Hata, K. A Stretchable Carbon Nanotube Strain Sensor for Human-Motion Detection. *Nat. Nanotechnol.* **2011**, *6*, 296−301.

(11) Pang, C.; Lee, G.-Y.; Kim, T.-i.; Kim, S. M.; Kim, H. N.; Ahn, S.-H.; Suh, K.-Y. A Flexible and Highly Sensitive Ttrain-gauge Sensor Using Reversible Interlocking of Nanofibres. *Nat. Mater.* **2012**, *11*, 795−801.

(12) Schwartz, G.; Tee, B. C.-K.; Mei, J.; Appleton, A. L.; Kim, D. H.; Wang, H.; Bao, Z. Flexible Polymer Transistors with High Pressure Sensitivity for Application in Electronic Skin and Health Monitoring. *Nat. Commun.* **2013**, *4*, 1859.

(13) Gong, S.; Schwalb, W.; Wang, Y.; Chen, Y.; Tang, Y.; Si, J.; Shirinzadeh, B.; Cheng, W. A Wearable and Highly Sensitive Pressure Sensor with Ultrathin Gold Nanowires. *Nat. Commun.* **2014**, *5*. (DOI:10.1038/ncomms4132).

(14) Lu, N.; Lu, C.; Yang, S.; Rogers, J. A. Highly Sensitive Skin-Mountable Strain Gauges Based Entirely on Elastomers. *Adv. Funct. Mater.* **2012**, *22*, 4044−4050.

(15) Jeong, J. W.; Yeo, W. H.; Akhtar, A.; Norton, J. J.; Kwack, Y. J.; Li, S.; Jung, S. Y.; Su, Y.; Lee, W.; Xia, J.; Cheng, H.; Huang, Y.; Choi, W.; Bretl, T.; Rogers, J. A. Materials and Optimized Designs for Human-Machine Interfaces Via Epidermal Electronics. *Adv. Mater.* **2013**, *25*, 6839−6846.

(16) Lee, J.; Kwon, H.; Seo, J.; Shin, S.; Koo, J. H.; Pang, C.; Son, S.; Kim, J. H.; Jang, Y. H.; Kim, D. E.; Lee, T. Conductive Fiber-Based Ultrasensitive Textile Pressure Sensor for Wearable Electronics. *Adv. Mater.* **2015**, *27*, 2433−2439.

(17) Barlian, A. A.; Park, W.-T.; Mallon, J. R.; Rastegar, A. J.; Pruitt, B. L. Review: Semiconductor Piezoresistance for Microsystems. *Proc. IEEE* **2009**, *97*, 513−552.

(18) Herrmann, J.; Müller, K.-H.; Reda, T.; Baxter, G.; Raguse, B.; De Groot, G.; Chai, R.; Roberts, M.; Wieczorek, L. Nanoparticle films as Sensitive Strain Gauges. *Appl. Phys. Lett.* **2007**, *91*, 183105.

(19) Farcau, C.; Sangeetha, N. M.; Moreira, H.; Viallet, B. t.; Grisolia, J.; Ciuculescu-Pradines, D.; Ressier, L. High-Sensitivity Strain Gauge Based on a Single Wire of Gold Nanoparticles Fabricated by Stop-and-Go Convective Self-Assembly. *ACS Nano* **2011**, *5*, 7137−7143.

(20) Gong, S.; Lai, D. T.; Su, B.; Si, K. J.; Ma, Z.; Yap, L. W.; Guo, P.; Cheng, W. Highly Stretchy Black Gold E-Skin Nanopatches as Highly Sensitive Wearable Biomedical Sensors. *Adv. Elect. Mater.* **2015**, *1*. (DOI: 10.1002/aelm.201400063).

(21) Amjadi, M.; Pichitpajongkit, A.; Lee, S.; Ryu, S.; Park, I. Highly Stretchable and Sensitive Strain Sensor Based on Silver Nanowire−Elastomer Nanocomposite. *ACS Nano* **2014**, *8*, 5154−5163.

(22) Xiao, X.; Yuan, L.; Zhong, J.; Ding, T.; Liu, Y.; Cai, Z.; Rong, Y.; Han, H.; Zhou, J.; Wang, Z. L. High-Strain Sensors Based on ZnO Nanowire/Polystyrene Hybridized Flexible Films. *Adv. Mater.* **2011**, *23*, 5440−5444.

(23) Tang, Y.; Gong, S.; Chen, Y.; Yap, L. W.; Cheng, W. Manufacturable Conducting Rubber Ambers and Stretchable Conductors from Copper Nanowire Aerogel Monoliths. *ACS Nano* **2014**, *8*, 5707−5714.

(24) Cohen, D. J.; Mitra, D.; Peterson, K.; Maharbiz, M. M. A Highly Elastic, Capacitive Strain Gauge Based on Percolating Nanotube Networks. *Nano Lett.* **2012**, *12*, 1821−1825.

(25) Boland, C. S.; Khan, U.; Backes, C.; O'Neill, A.; McCauley, J.; Duane, S.; Shanker, R.; Liu, Y.; Jurewicz, I.; Dalton, A. B.; Coleman, J. N. Sensitive, High-Strain, High-Rate Bodily Motion Sensors Based on Graphene-Rubber Composites. *ACS Nano* **2014**, *8*, 8819−8830.

(26) Wang, Y.; Wang, L.; Yang, T.; Li, X.; Zang, X.; Zhu, M.; Wang, K.; Wu, D.; Zhu, H. Wearable and Highly Sensitive Graphene Strain Sensors for Human Motion Monitoring. *Adv. Funct. Mater.* **2014**, *24*, 4666−4670.

(27) Yan, C.; Wang, J.; Kang, W.; Cui, M.; Wang, X.; Foo, C. Y.; Chee, K. J.; Lee, P. S. Highly Stretchable Piezoresistive Graphene-Nanocellulose Nanopaper for Strain Sensors. *Adv. Mater.* **2014**, *26*, 2022−2027.

(28) Bae, S.-H.; Lee, Y.; Sharma, B. K.; Lee, H.-J.; Kim, J.-H.; Ahn, J.-H. Graphene-Based Transparent Strain Sensor. *Carbon* **2013**, *51*, 236−242.

(29) Hempel, M.; Nezich, D.; Kong, J.; Hofmann, M. A Novel Class of Strain Gauges Based on Layered Percolative Films of 2D Materials. *Nano Lett.* **2012**, *12*, 5714−5718.

(30) Takei, K.; Yu, Z.; Zheng, M.; Ota, H.; Takahashi, T.; Javey, A. Highly Sensitive Electronic Whiskers Based on Patterned Carbon Nanotube and Silver Nanoparticle Composite Films. *Proc. Natl. Acad. Sci. U. S. A.* **2014**, *111*, 1703−1707.

(31) Lee, C.; Jug, L.; Meng, E. High Strain Biocompatible Polydimethylsiloxane-Based Conductive Graphene and Multiwalled Carbon Nanotube Nanocomposite Strain Sensors. *Appl. Phys. Lett.* **2013**, *102*, 183511.

(32) Hwang, S.-H.; Park, H. W.; Park, Y.-B. Piezoresistive Behavior and Multi-Directional Strain Sensing Ability of Carbon Nanotube−

DOI: 10.1021/acsami.5b05001
ACS Appl. Mater. Interfaces 2015, 7, 19700−19708

Graphene Nanoplatelet Hybrid Sheets. *Smart Mater. Struct.* **2013**, *22*, 015013.
(33) Lee, S.; Shin, S.; Lee, S.; Seo, J.; Lee, J.; Son, S.; Cho, H. J.; Algadi, H.; Al-Sayari, S.; Kim, D. E.; Lee, T. Ag Nanowire Reinforced Highly Stretchable Conductive Fibers for Wearable Electronics. *Adv. Funct. Mater.* **2015**, *25*, 3114.
(34) Chen, Y.; Ouyang, Z.; Gu, M.; Cheng, W. Mechanically Strong, Optically Transparent, Giant Metal Superlattice Nanomembranes from Ultrathin Gold Nanowires. *Adv. Mater.* **2013**, *25*, 80−85.
(35) Huo, Z.; Tsung, C.-k.; Huang, W.; Zhang, X.; Yang, P. Sub-Two Nanometer Single Crystal Au Nanowires. *Nano Lett.* **2008**, *8*, 2041−2044.
(36) Feng, H.; Yang, Y.; You, Y.; Li, G.; Guo, J.; Yu, T.; Shen, Z.; Wu, T.; Xing, B. Simple and Rapid Synthesis of Ultrathin Gold Nanowires, their Self-assembly and Application in Surface-Enhanced Raman Scattering. *Chem. Commun.* **2009**, *15*, 1984−1986.
(37) Khang, D.-Y.; Jiang, H.; Huang, Y.; Rogers, J. A. A Stretchable Form of Single-Crystal Silicon for High-Performance Electronics on Rubber Substrates. *Science* **2006**, *311*, 208−212.
(38) Lewis, J. Material Challenge for Flexible Organic Devices. *Mater. Today* **2006**, *9*, 38−45.

DOI: 10.1021/acsami.5b05001
ACS Appl. Mater. Interfaces 2015, 7, 19700−19708